A&A 374, 443–453 (2001)
DOI: 10.1051/0004-6361:20010739

Astronomy & Astrophysics

Probing the faint end of the Galaxy luminosity function at $z = 3$ with Lyα emission*

J. U. Fynbo[1], P. Møller[1], and B. Thomsen[2]

[1] European Southern Observatory, Karl-Schwarzschild-Straße 2, 85748 Garching, Germany
[2] Institute of Physics and Astronomy, Århus University, 8000 Århus C., Denmark

Received 15 March 2001 / Accepted 21 May 2001

Abstract. We present spectroscopic observations obtained with the ESO Very Large Telecope (VLT) of seven candidate Lyα emitting galaxies in the field of the radio quiet Q1205-30 at $z = 3.04$ previously detected with deep narrow band imaging. Based on equivalent widths and limits on line ratios we confirm that all seven objects are Lyα emitting galaxies. Deep images also obtained with the VLT in the B and I bands show that five of the seven galaxies have very faint continuum fluxes (I(AB) $\approx$ 26.8 and B(AB) $\approx$ 27.3). The star formation rates of these seven galaxies estimated from the rest-frame UV continuum around 2000 Å, as probed by the I-band detections, as well as from the Lyα luminosities, are 1–4 $M_\odot$ yr^{-1} assuming a Hubble constant of 65 km s^{-1} Mpc^{-1}, $\Omega_m = 0.3$, and $\Omega_\Lambda = 0.7$. This is 1–3 orders of magnitude lower than for other known populations of star-forming galaxies at similar redshifts (the Lyman-Break galaxies and the sub-mm selected sources). The inferred density of the objects is high, 16 ± 4 per arcmin^2 per unit redshift. This is consistent with the integrated luminosity function for Lyman-Break galaxies down to $R = 27$ if the fraction of Lyα emitting galaxies is $\approx$70% at the faint end of the luminosity function. However, if this fraction is 20% as reported for the bright end of the luminosity function then the space density in this field is significantly larger (by a factor of 3.5) than expected from the luminosity function for Lyman-Break galaxies in the HDF–North. This would be an indication that at least some radio quiet QSOs at high redshift reside in overdense environments or that the faint end slope of the high redshift luminosity function has been underestimated. We find evidence that the faint Lyα galaxies are essentially dust–free. These observations show that Lyα emission is an efficient method by which to probe the faint end of the luminosity function at high redshifts.

Key words. galaxies: formation – quasars: absorption lines – quasars: individual: Q1205-30

1. Introduction

During the last ten years the amount of observational data neccessary for understanding galaxy formation at high redshift has increased from almost nothing to a stage where of order a thousand galaxies has been detected in emission and confirmed spectroscopically. The bulk of these galaxies has been selected by use of the Lyman-break colour selection technique (Steidel & Hamilton 1992; Steidel et al. 1996; Adelberger & Steidel 2000) and later been spectroscopically confirmed. For the Lyman-break galaxies (LBGs) it is important to keep in mind that only those brighter than the "spectroscopic limit" (R(AB) $\lesssim$ 25.5) may have their redshifts confirmed, unless a Lyα emission line is present. The spectroscopically confirmed LBGs (SLBGs) have star formation rates similar to local starburst galaxies. The brightest end of the high redshift LBG luminosity function (LF) is therefore well determined, while the faint end is based on photometric redshifts and significant corrections for incompleteness. One may improve the photometric redshift selection by inclusion of infrared colours (e.g. Fontana et al. 2000 and references therein). A second selection technique for high redshift galaxies is selection by means of sub-mm emission. This technique is at present only sensitive to galaxies with star-formation rates exceeding 10^3 $M_\odot$ yr^{-1} (e.g. Ivison et al. 2000). Independent of their emission properties, objects found at high redshifts as Damped Lyman-α Absorbers (DLAs) in the spectra of background QSOs are likely related to galaxies or to galaxies in the process of assembly. DLAs are in current models of galaxy formation found to trace the collapsed regions near intersections of dark-matter filaments where galaxies form

Send offprint requests to: J. U. Fynbo, e-mail: jfynbo@eso.org
* Based on observations made with ESO Telescopes at the Paranal Observatory under programme ID 64.O-0187.

(e.g. Rauch et al. 1997). Furthermore, DLAs are chemically enriched implying that star-formation is or has been going on nearby.

Several studies have shown that Lyα narrow-band imaging is an alternative technique to identify high redshift galaxies (Møller & Warren 1993; Francis et al. 1995; Pascarelle et al. 1996; Pascarelle et al. 1998; Cowie & Hu 1998; Hu et al. 1998; Fynbo et al. 1999, 2000; Kudritzki et al. 2000; Kurk et al. 2000; Pentericci et al. 2000; Steidel et al. 2000; Roche et al. 2000; Rhoads et al. 2000). So far it has not been considered efficient enough to seriously compete with the LBG technique, but it does have the advantage that spectroscopic confirmation is not limited by the broad band flux. Most recently the current success in identification of Gamma-Ray Bursts at high redshifts, has provided a completely independent selection technique for the host galaxies of Gamma-Ray Bursts (e.g. Odewahn et al. 1998; Bloom et al. 1999; Holland & Hjorth 1999; Vreeswijk et al. 2000; Smette et al. 2001; Jensen et al. 2001; Fynbo et al. 2001).

From the point of view of observations, what is still missing is an understanding of the connection between high redshift galaxies selected in different ways. Fontana et al. (2000) find that photometric redshifts including IR colours select nearly a factor of 2 more high redshift galaxy candidates in the Hubble Deep Fields (HDFs) than pure LBG photometric selection does, to the same flux limits. However, this discrepancy cannot be resolved spectroscopically. While LBGs are selected by continuum flux, DLAs are selected by gas cross-section. Under the assumption of a scaling relation between the gas disc size and the luminosity for high redshift galaxies, and by normalising this relation using the few observed impact parameters for $z \approx 3$ DLAs, DLAs are predicted to be much fainter than the SLBG limit (Fynbo et al. 1999; Haehnelt et al. 2000; see also Ellison et al. 2001). Members of the population of galaxies producing DLAs are obviously not only found close to QSO lines of sight so we expect an abundant population of galaxies below the current spectroscopic limit for LBGs.

From a theoretical point of view, the properties of this faint end of the high redshift LF is important in order to constrain the importance of stellar feedback processes (e.g. Efstathiou 2000; Thacker & Couchman 2000; Poli et al. 2001) and the fraction of the background of hydrogen ionising photons produced by high mass stars at high redshift (Steidel et al. 2001; Haehnelt et al. 2001).

To probe the faint end of the LF at high redshifts we need methods to search for emission from high redshift galaxies fainter than $R \lesssim 25.5$. Here several methods are possible: *i*) Using the Lyman break technique and photometric redshifts, LFs for $z = 3$ galaxies has been presented by Adelberger & Steidel (2000) and by Poli et al. (2001) down to $R = 27$. The faint end ($R > 25.5$) of these LFs are uncertain due to the lack of spectroscopic confirmation, *ii*) Lyα narrow–band imaging. *iii*) Imaging of DLAs at very faint continuum levels with the *Hubble Space Telescope* (Møller & Warren 1998; Kulkarni et al. 2000, 2001; Ellison et al. 2001; Warren et al. 2001; Møller et al. 2001 in prep.), and *iv*) deep searches for the host galaxies of well-localized (to within a fraction of an arcsec using the positions of optical transients) Gamma-Ray Bursts. In this paper we focus on Lyα emission as a method by which to study the faint end of the LF at $z = 3$.

In Fynbo et al. (2000, Paper I) we reported on six faint candidate Lyα Emitting Galaxies detected in a very deep narrow band image of the $z = 3.036$ radio quiet QSO Q1205-30 obtained with the NTT. Here we present photometric and spectroscopic follow-up observations of these 6 candidates (called S7–S12, detected at better than 5σ) plus 2 marginal candidates (S13 and S14, detected at the $\approx 4\sigma$ level). This paper is concerned mostly with the details of the observations, data reduction and the results concerning the physical properties of the Lyα galaxies. In a separate *Letter* we discussed the spatial distribution of the confirmed Lyα galaxies and how it related to current models of structure formation in the early universe (Møller & Fynbo 2001). In that paper we concluded that the Lyα emitting objects are proto-galatic sub-units in the process of assembly, and for that reason chose to refer to them as "Lyα Emitting Galaxy-building Objects" (LEGOs). Here, for consistency, we shall adopt the same acronym. The rest of the paper is organized as follows: In Sect. 2 we describe the observations and the data reduction, in Sect. 3 we present our results, in Sect. 4 we discuss our results in terms of star–formation rates and luminosity function compared to that of the LBGs and in Sect. 5 we summarise our conclusions. Throughout this paper we adopt a Hubble constant of 65 km s^{-1} Mpc^{-1} and assume $\Omega_m = 0.3$ and $\Omega_\Lambda = 0.7$.

2. Observations and data reduction

2.1. Preimaging and construction of masks

For the spectroscopy we used the Multi Object Spectroscopy (MOS) mode of FORS1 on the VLT–UT1 telescope. Pre–imaging for MOS was obtained in Service Mode during two nights in January 2000, well ahead of our Visitor Mode run, and consisted of 13 exposures each of 400sec in the Bessel B-filter. The 5σ detection limit of the final combined pre–image was $B(\mathrm{AB}) = 26.7$. Surprisingly this did not, however, allow the detection of continuum emission from all of the eight target objects S7-S14 (see Sect. 3.2 below). Furthermore, for one of those objects (S9) where we *did* detect continuum emission, there was a small but significant offset between the continuum position and the narrow–band position on the sky. For each of the eight target objects we therefore derived local transformations between the NTT narrow–band image and the VLT B–band image, and placed artificial stars at the positions in the VLT image corresponding to the positions of S7-S14 in the NTT narrow–band image. Two of us did this independently and found positions that agreed to within 1/3 of a FORS1 pixel, corresponding to 0.07 arcsec. To minimize slitlosses, which could become severe if our

Table 1. The log of VLT observations.

date	setup	seeing arcsec	Exposure time (sec)
Imaging:			
2000 Jan. 12, 17	Bessel B	0.68–1.02	5200
2000 Mar. 5	Bessel I	0.55–0.75	3750
Spectroscopy:			
2000 Mar. 5	MOS, maskB1	0.78–0.96	7200
2000 Mar. 4	MOS, maskB2	0.78–1.18	7200
2000 Mar. 4	MOS, maskB3	0.61–0.66	7200
2000 Mar. 4	MOS, maskR1	0.77–0.93	5400
2000 Mar. 5	MOS, maskR2	0.57, 0.78	3600
2000 Mar. 5	MOS, maskR3	0.59–0.95	5400

invisible objects were not perfectly centered in the slitlets, and/or if the objects were extended in Lyα, we chose to use a slit–width of 1.2 arcsec for all slitlets.

We chose grism G600B to cover the region of Lyα at $z = 3.036$ and grism G600R to look for other emission lines at longer wavelengths. Even though we did not expect to see any lines in the red spectra, it is imperative that they are deep enough that we can rule out the alternative interpretation that our objects are O II emitters rather than Lyα emitters. G600B has a wavelength coverage from 3600 Å to 6000 Å (depending somewhat on the position on the CCD) and a spectral resolution of 815 whereas G600R covers the range 5200 Å–7400 Å at a spectral resolution of 1230.

We constructed three independent masks. In addition to covering all eight candidate LEGOs, several of them in more than one mask, this also allowed us to obtain spectra of objects close to the quasar line of sight. For the mask construction we used the *FORS Instrumental Mask Simulator* (FIMS). We hereafter refer to the three G600B masks as maskB1, maskB2 and maskB3, and to the three G600R masks as maskR1, maskR2 and maskR3.

2.2. Spectroscopy and I-band imaging

The spectroscopic observations were carried out during the two nights of March 4–5 2000 under photometric and good seeing conditions. We obtained total integration times of 4×1800 sec for each of maskB1–maskB3 and 3×1800 sec, 2×3600 sec and 3×1800 sec for maskR1, maskR2 and maskR3 respectively. As the seeing *fwhm* for all frames was significantly smaller than the slit-width the spectral resolution is determined by the seeing and/or the size of the object. We also obtained 15×250 sec images in the Bessel I–band filter. During the G600B observations the CCD was binned 2×2 in order to reduce the influence of read-out noise. For all spectroscopic observations the CCD was read out in single port, high gain mode. For the imaging observations the CCD was read out using the four port, high gain mode. The journal of observations appears as Table 1.

2.3. Data reduction

The pre–imaging B–band images and the I–band images were BIAS subtracted and flat–fielded using standard techniques and the individual reduced images were combined using the σ–clipping algorithm described in Møller & Warren (1993). The combined images reach $5(2)\sigma$ detection limits in 1 arcsec^2 circular apertures of 25.9(26.9) in the I–band and 26.7(27.7) in the B–band (both in the AB-system).

The spectroscopic frames were first BIAS subtracted. The flat-fielding was thereafter done in the following way. First we median filtered the flat-fields along the dispersion direction (x-axis) using a 30×1 boxcar filter for the G600B flat-frames and a 60×1 boxcar filter for the G600R flat-frames. Then we normalised the flat-frames by dividing the unfiltered flat-frames with the filtered flat-frames. Finally, we divided the science frames with these normalised flat-frames. The individual BIAS subtracted and flat-fielded science spectra were subsequently sky-subtracted in the following way. First we removed cosmic ray hits from the sky-region of the 2-dimensional spectrum by σ-clipping along each spatial direction column. We determined a 2-dimensional sky-frame using the *background* task in the *kpnoslit* package in IRAF. This sky-frame was then subtracted from the original BIAS subtracted and flat-fielded 2-dimensional science spectrum. The individual reduced and sky-subtracted science spectra were then combined using σ-clipping for rejection of cosmic ray hits.

1-dimensional spectra were extracted using the *apall* task. For objects without or with very faint continuum we used bright objects from neighbour slitlets to determine the trace of the spectra.

The 1-dimensional spectra were wavelength calibrated using the *dispcor* task. The rms of the deviations from the fits to 3. order chebychev polynomia were 0.3–0.5 Å for the G600B spectra and 0.05–0.1 Å for the G600R spectra. The high rms values for the wavelength calibration of the G600B spectra is due to the binning of CCD for the G600B spectra which imply fewer pixels per resolution element.

3. Results

3.1. Spectroscopy

3.1.1. Emission line candidates and line fluxes

Our candidate list consisted of six "certain" candidates (Lyα $S/N > 5$) named S7–S12 and two "possible" candidates (Lyα $S/N \approx 4$) named S13 and S14. The candidates were selected on the basis of excess flux in the narrow–band as compared to their B and I band magnitudes (see Paper I). A Lyα emission line was detected spectroscopically for all objects except S14. The non–confirmation of S14 is consistent with the new and deeper B–band image also obtained during this run (Sect. 3.2), as the detection of B–band continuum for S14 lowered the significance of the narrow–band excess below 3σ.

Table 2. Properties of the confirmed LEGOs S7–S13. Magnitudes are measured in a 3.5 arcsec diameter aperture. Two Lyα fluxes are given, one as measured through the slit (flux(slit)) and one corrected to the 3.5 arcsec aperture (flux(aper) see text for details). The errors on the linefluxes are propagated errors from photon statistics relevant for determining the significanse of the detection, they do not include calibration errors which are estimated to be 30% because of the large aperture correction.

Source	wavelength (Å)	redshift	*fwhm* (Å)	velocity width km s^{-1}	B mag	I mag	flux(slit)$\times 10^{17}$ erg s^{-1} cm^{-2}	flux(aper)$\times 10^{17}$ erg s^{-1} cm^{-2}	$W_{\rm obs}$ (Å)
S7	4911.6	3.0402	7.4	<350	25.61 ± 0.11^a	24.28 ± 0.09^a	1.04 ± 0.15	1.58 ± 0.23	> 61
S8	4911.1	3.0398	6.5	<240	$\sim 27.3^b$	$\sim 26.8^b$	1.70 ± 0.18	2.58 ± 0.27	456^b
S9	4905.2	3.0350	7.2	<340	25.36 ± 0.07	24.61 ± 0.13	3.51 ± 0.18	5.34 ± 0.27	> 164
S10	4905.6	3.0353	7.2	<240	$\sim 27.3^b$	$\sim 26.8^b$	2.09 ± 0.26	3.17 ± 0.40	456^b
S11	4900.6	3.0312	7.2	<440	$\sim 27.3^b$	$\sim 26.8^b$	1.48 ± 0.26	2.25 ± 0.40	456^b
S12	4903.2	3.0333	8.2	<520	$\sim 27.3^b$	$\sim 26.8^b$	1.54 ± 0.31	2.34 ± 0.48	456^b
S13	4890.4	3.0228	7.3	<450	$\sim 27.3^b$	$\sim 26.8^b$	1.39 ± 0.19	2.11 ± 0.29	456^b

[a] Including the nearby red object to the West of S7 proper.
[b] Measured in the median image of S8, S10–S13.

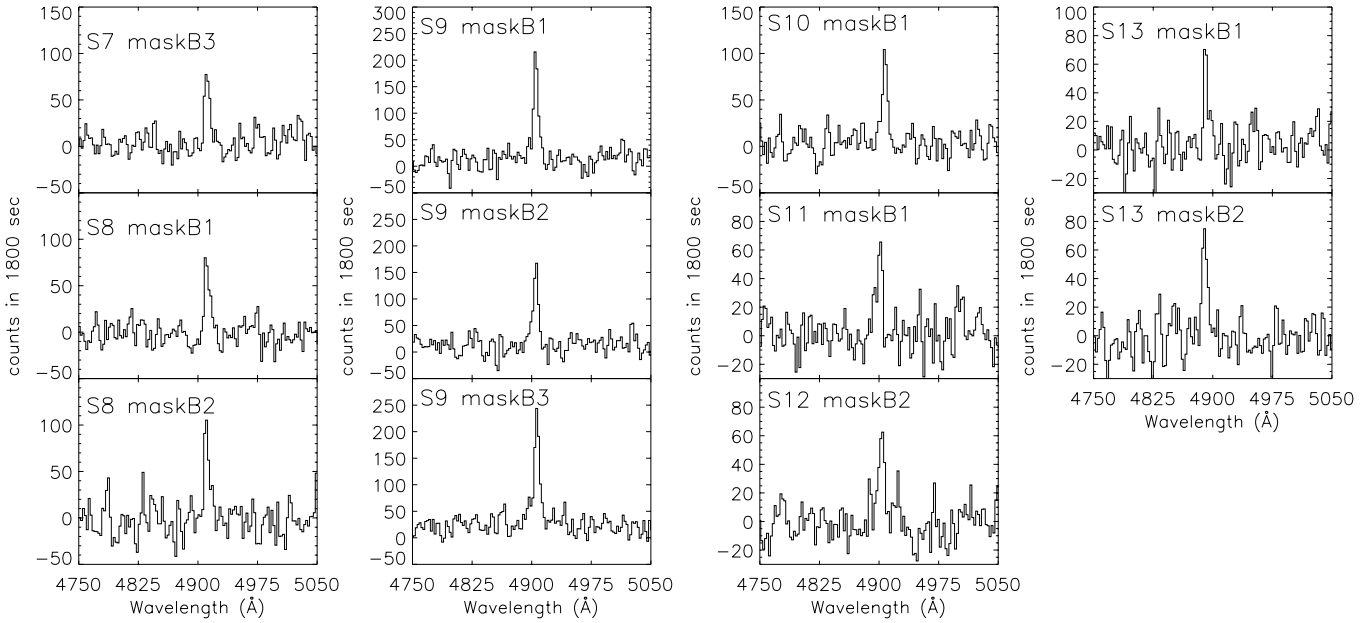

Fig. 1. The spectral regions around the Lyα emission lines for the LEGOs S7–S13. For S8, S9, and S13 we show the spectra from several masks. As seen, the presence of emission lines is confirmed for all 7 candidates. For S14 (not shown) we did not detect an emission-line within the range of the narrow filter.

In Fig. 1 we show extractions of the blue grism spectra of all the candidates for which we confirm the presence of an emission line within the transmission curve of the narrow filter. Only for S7 and S9 did we detect a faint continuum in the spectra.

With variable seeing and 1.2 arcsec slits it was not possible to obtain a spectrophotometric calibration. Nevertheless we obtained a rough calibration as follows. For each mask we had placed several slits on stars for which we had accurate B and I magnitudes. For the G600B masks we selected a star with a flat spectrum in B, and used that as a local standard for the flux calibration of emission lines. The calibration was done for each mask individually, and the results were combined afterwards for those objects that were observed more than once. The scatter for the objects observed more than once was about two–three times larger than the observational errors, confirming that this calibration is dominated by slit–losses as we expected. The resulting line fluxes are given in Table 2 (flux(slit)).

The flux calibration described above is only valid if all the emission line objects are point sources. For extended objects the slit–losses will be larger than for the standard star, and an additional aperture correction must be applied. Comparing to the imaging line fluxes found with a circular aperture of diameter 3.5 arcsec (Paper I), we

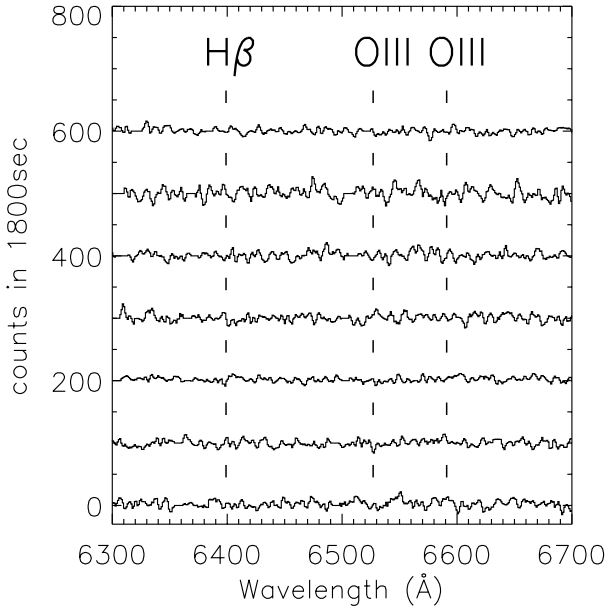

Fig. 2. Shown here are parts of the G600R spectra were Hβ and O III lines would have been if the emission line detected with the narrow–band imaging (Paper I) were due to O II at $z = 0.31$. S7 is at the bottom and S13 at the top. The spectra have been smoothed with a seven pixel (7.4 Å) box car filter. For S8, S9 and S13 the spectra are the average of 2, 3, and 2 spectra respectively.

find a mean aperture correction of 0.46 mag. Line fluxes including this mean aperture correction are also given in Table 2 (flux(aper)).

3.1.2. Identifications and redshifts

Before we can conclude that the emission lines are indeed due to Lyα at $z \approx 3.04$, we must first exclude any possible low redshift "contamination". In the deep narrow band imaging discussed by Kudritzki et al. (2000) 9 of 10 candidates were confirmed as Lyα emitters at $z = 3.1$, while the last proved to be a galaxy at $z = 0.35$ where the O II 3727 Å line fell in the same narrow–band filter. There are other, albeit less likely, possible identifications (Mg II and Ne III). Those can all be tested by searching for additional emission lines (O II, Hβ and especially O III). For most of the possible interpretations the O III would be redshifted out of the G600B spectra. For this reason we also obtained spectra of all objects with the G600R grism.

For none of the confirmed emission–line objects S7–S13 did we detect any other emission line, neither in the G600B nor in the G600R spectra. In Fig. 2 we show the regions of the G600R spectra where the Hβ and O III lines would have fallen if the emission lines seen in Fig. 1 had been O II at $z = 0.313$ (S7 at the bottom and S13 at the top). The spectra have been smoothed by a 7 pixel (7.4 Å) boxcar filter and regions with large errors due to strong sky-lines were set to zero. As seen, Hβ and O III lines are not present in any of the spectra. The question of possible alternatives to the Lyα identification is an important one, and we shall return to a complete discussion in Sect. 4.1. For now we shall assume that the lines are indeed due to Lyα.

The wavelengths and widths of the emission lines were determined by fitting them with Gaussian profiles. The uncertainty in the determination of the wavelength centroid is about 0.3 Å. The results are given in Table 2 where we also list the resulting redshifts under the assumption that the lines are due to Lyα.

In order to constrain the intrinsic width of the lines we must know the spectroscopic resolution. An upper limit to the *fwhm* of the resolution profile along the dispersion direction can be obtained from the width of the slitlets and the dispersion. With a slit width of 1.2 arcsec (3 pixels) and dispersion of 2.4 Å per pixel the resolution would have been about 7.2 Å if the seeing had been worse than 1.2 arcsec. However, as the seeing was in all cases significantly better than 1.2 arcsec the spectroscopic resolution is smaller than 7.2 Å *fwhm*. An upper limit to the spectroscopic resolution can be derived from the spatial profile of the spectra of point sources at wavelengths near 4900 Å. Converted to Å the spatial widths are 5.9 Å, 5.7 Å and 4.8 Å for maskB1, maskB2 and maskB3 respectively. As the instrumental resolution for FORS is slightly lower along the dispersion direction than along the spatial direction (T. Szeifert, private communication) these values can be used as lower limits on the spectroscopic resolution. From this lower limit we can obtain upper limits to the intrinsic widths of the lines by deriving the intrinsic widths that convolved with a Gaussian with a width corresponding to the lower limit on the spectroscopic resolution reproduces the observed line widths. These upper limits are also given in Table 2. The line widths are smaller than 6 Å or 370 km s^{-1} for Lyα at $z = 3.04$.

3.2. Imaging

Figure 3 and the two left panels in Fig. 4 show regions of size 12×12 arcsec^2 centred on each of the objects S7–S12 and S13–S14 from the combined NTT narrow–band image (top row), VLT B–band image (middle row) and VLT I–band image (bottom row). Only two of the objects, S7 and S9, are detected above our 2σ detection limits of $I(\mathrm{AB}) = 26.9$ and $B(\mathrm{AB}) = 27.7$ (detection limits for 1 arcsec^2 circular apertures). Those two galaxies were already detected in the deep NTT images presented in Paper I. For S9 both the B–band and I–band emission is centred 0.51 ± 0.05 arcsec south of the narrow-band position. In the broad band images of S7 we see two nearby objects. The center of the Lyα emission is found 0.21 ± 0.11 arcsec east of the easternmost of the two, which we identify as the likely host of the Lyα emission. We cannot be certain that the nearby western object is unrelated, hence the aperture magnitudes for S7 given in Table 2 includes both of the objects. The not–confirmed ($< 5\sigma$) candidate S14 is clearly detected in both the B and I bands.

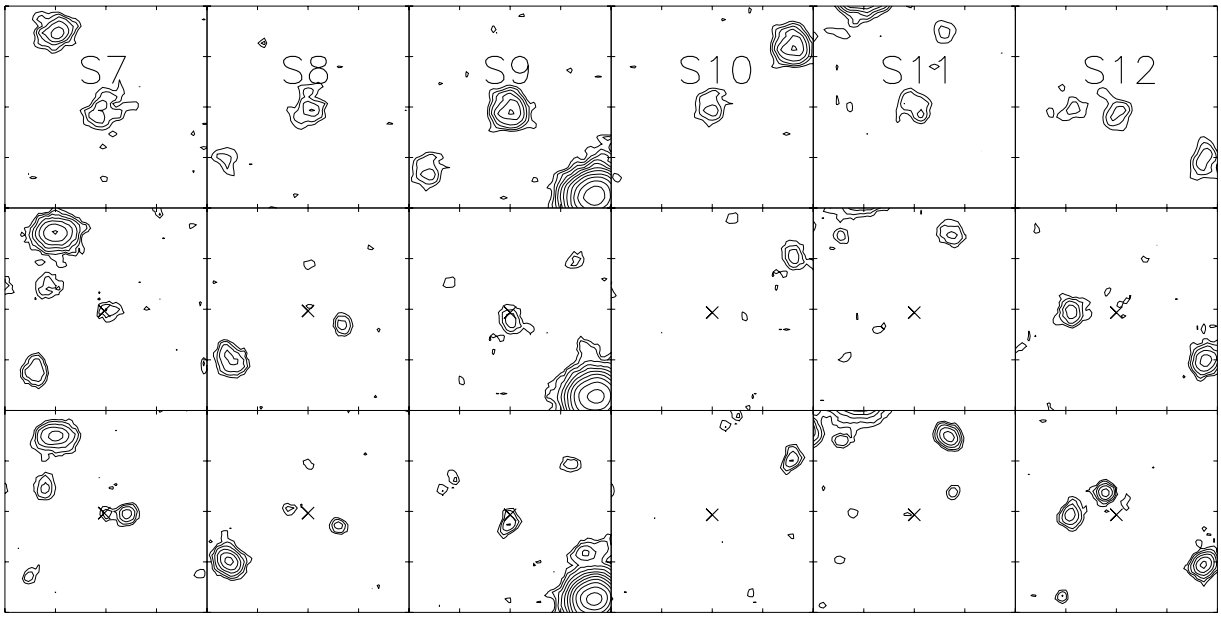

Fig. 3. Contour plots of the combined NTT narrow–band (top), VLT B–band (middle) and VLT I–band (bottom) images for each of the six candidate emission line galaxies S7–S12 detected with $S/N > 5$ in the NTT narrow–band image (Paper I). The size of the individual fields is 12×12 arcsec^2 and the fields are orientated with east to the left and north up. The contour levels are logarithmic.

The B magnitude is bright enough to confirm that the apparent narrow–band excess in the old data set was not significant.

For the five remaining objects we detect no broad band flux above 2σ. In order to constrain the limit on the broad band emission further we registered the sub–images of the objects S8, S10–S13 to the centroids of their Lyα emission and coadded them. In the right panel of Fig. 4 we show the median of the coadded images. We now detect a faint object in both the I–band and the B–band. To be able to compare the fluxes we apply aperture corrections determined from a bright point source and arrive at $I(\mathrm{AB}) = 26.8 \pm 0.3$ and $B(\mathrm{AB}) = 27.3 \pm 0.2$ for the 3.5 arcsec diameter circular aperture.

If this flux was due mainly to one or two of the objects, they would have been visible on the individual images. Hence, we conclude that the flux must be fairly evenly distributed on most or all of the five objects, and that they each must have roughly the magnitudes measured in the combined images. It is interesting to note that unlike S7 and S9, the continuum emission in the coadded frames is centered on the same position as the Lyα emission. This suggests that the relatively bright continuum object identified as S9 and the two–component object identified as S7 are, at least partly, due to a chance alignment of unrelated objects. Hence, the broad–band magnitudes given for S7 and S9 should probably be regarded as upper limits on their brightness.

Møller & Warren (1998) reported that on HST images of three Lyα emitting objects related to the DLA at $z = 2.81$ in front of PKS0528–250, there was evidence that the Lyα emission was significantly more extended than the continuum sources. We measured the *FWHM* of the Lyα emission of S9 and of the stacked Lyα object, and found an intrinsic size (after correcting for the seeing) of 0.98 and 0.65 arcsec (*FWHM*). This supports the result reported by Møller & Warren (1998).

4. Discussion

4.1. Line identification

We now return in more detail to the identification of the detected emission lines. For a discussion of ways to discriminate between Lyα and lower redshift objects for single emission lines around 8000–9000 Å, corresponding to very high redshifts ($z \gtrsim 5$) for Lyα, see Stern et al. (2000). Here we discuss possible contaminants for $z = 3$ Lyα emitters.

Mg II and Ne III can both be excluded easily since in this case we would have detected the stronger O II line. In the following we will discuss how to reject the possibility that the observed line is due to O II. There are two independent ways to check the likelyhood of the identification as Lyα rather than O II. One is by its equivalent width, the other by upper limits on line flux ratios. We shall here apply both tests, and as reference point for the low redshift identification we have chosen the large sample of emission line galaxies from the survey of Terlevich et al. (1991).

4.1.1. Equivalent widths

The expected rest equivalent width of unextinguished star formation induced Lyα can be as high as 200–300 Å (Charlot & Fall 1993; Valls–Gabaud 1993), which at a

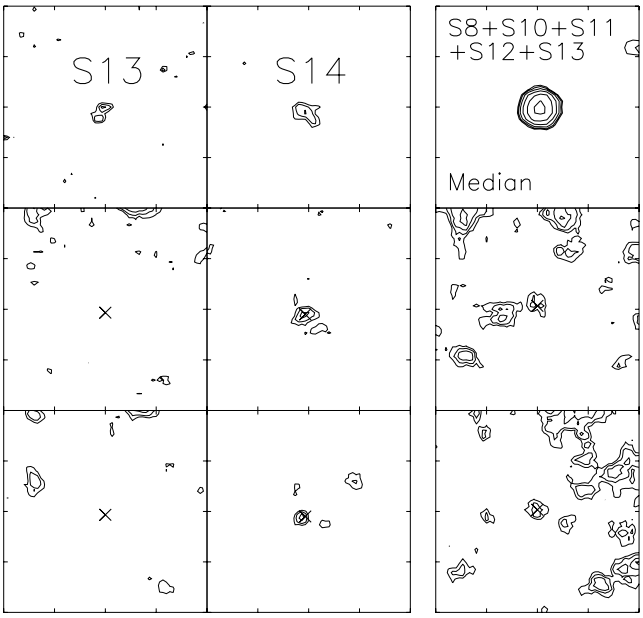

Fig. 4. *Two left panels*: Contour plots of the combined NTT narrow–band (top), VLT B–band (middle) and VLT I–band (bottom) images for the two candidate emission line galaxies S13 and S14 detected with $S/N < 5$ in the NTT narrow–band image. The size of the individual fields is $12{\times}12$ arcsec^2 (as in Fig. 3) *Right panel*: Same as Fig. 3 and the two left panels, but for the median image of S8, S10–S13 and with different contour levels. Broad band emission is detected in the median images at the exact position of the stacked narrow–band object.

redshift of 3 would result in an observed equivalent width of order 1000 Å. Even with a fair amount of absorption by dust, the observed equivalent width would remain large.

The continuum of low redshift O II galaxies is, in contrast to that of the Lyα selected galaxies at high redshift, for the most part easily detected. In the sample of Terlevich et al. (1991) we find a median O II rest equivalent width of 59 Å, and the 95% quantile is 163 Å. In Table 2 we list the observed equivalent widths ($W_{\rm obs}$) of our lines. As discussed above, the broad–band aperture magnitudes of the two objects S7 and S9 probably include flux unrelated to the emission line objects, and hence the calculated equivalent widths are lower limits. For the remaining objects it was necessary to coadd the images before we were able to measure their broad–band flux. For consistency we list the equivalent width measured on the stacked images.

For an O II galaxy at $z = 0.31$ we would expect a median equivalent width of 77 Å and none of seven objects should be above the 95% quantile of 214 Å. This is incompatible with the observed distribution.

4.1.2. Line intensity ratios

In order to compare the intensity ratios, we first had to determine the upper limit for the non–detection of lines in the predicted region for O III and Hβ. For the flux calibration of the G600R spectra we used the exact same method as described in Sect. 3.1.1 for G600B. To maximixe the S/N for the non-detection of Hβ and O III emission lines, we stacked all the spectra. In Fig. 5a we show the stacked spectrum (middle panel), and we have marked the expected positions of various emission lines. We find 2σ upper limits to the log of flux ratios as follows: $\log(f_{\rm OIII}/f_{\rm OII}) < -0.92$, $\log(f_{\rm H\beta}/f_{\rm OII}) < -0.92$, and $\log(f_{\rm NeIII}/f_{\rm OII}) < -1.09$. Above the stacked spectrum we plot the spectrum of the quasar in order to show the positions of the Lyα and C IV emission lines. No C IV line is detected in the stacked spectrum. The flux ratio ($\log(f_{\rm CIV}/f_{\rm Ly\alpha}) < -0.92$) excludes a significant AGN contribution to the Lyα emission. Below the stacked spectrum we show for comparison the spectrum of an O II galaxy observed by chance during the same run in one of the slits we placed on random objects in order to fill the masks. This galaxy was observed at a redshift of $z({\rm O\,II}) = 0.224$, but we have shifted it to $z = 0.313$ for easy comparison.

In Terlevich et al. (1991) we only found data for the equivalent widths of their emission line sample. In order to convert those to intensity ratios of two lines, we need first to determine the ratio of the local continuum flux under those two lines. In all the published spectra of the Terlevich sample we therefore measured the ratio of the continuum flux at 3727–3870 Å (OII and NeIII) and at 5007 Å (OIII). We then determined the mean of this ratio and the maximum of the ratio (which is the worst case), and used both of them to convert the equivalent width ratios to flux ratios. The results are plotted in Fig. 5b. In Figs. 5b1, b2 we plot line flux ratios calculated from the mean continuum slope. The box and arrows in the lower left corner marks the 2σ upper limits of our non–detections. In Figs. 5b3, b4 we repeat the same plots, but here we have used the "worst case" continuum for the conversion to flux ratios. Even in this case our 2σ upper limits have no overlap with the O II galaxy distribution.

In summary of this section we have applied two independent methods (equivalent widths and line flux ratios) to test how well our sample of emission line objects would fit if interpreted as low redshift O II galaxies. Both tests reject the interpretation, and we conclude that all seven objects presented here are Lyα emitters at $z \approx 3.04$.

4.2. Star–formation rates

In Paper I we calculated star–formation rates (SFR) based on the Lyα fluxes. Here, for comparison, we calculate the SFRs from the continuum fluxes. As detailed in Sect. 3.2 we have reasons to believe that the continuum of S7 and S9 may be boosted by neighbour objects, therefore we perform the calculation for the remaining five objects only.

The restframe UV continuum in the range 1500 Å–2800 Å can be used as a SFR estimator if one assumes that the star-formation is continuous over a time scale of more than 10^8 years. Kennicutt (1998) provides the relation

$$\mathrm{SFR}(M_\odot\ \mathrm{yr}^{-1}) = 1.4 \times 10^{-28} \times L_\nu,$$

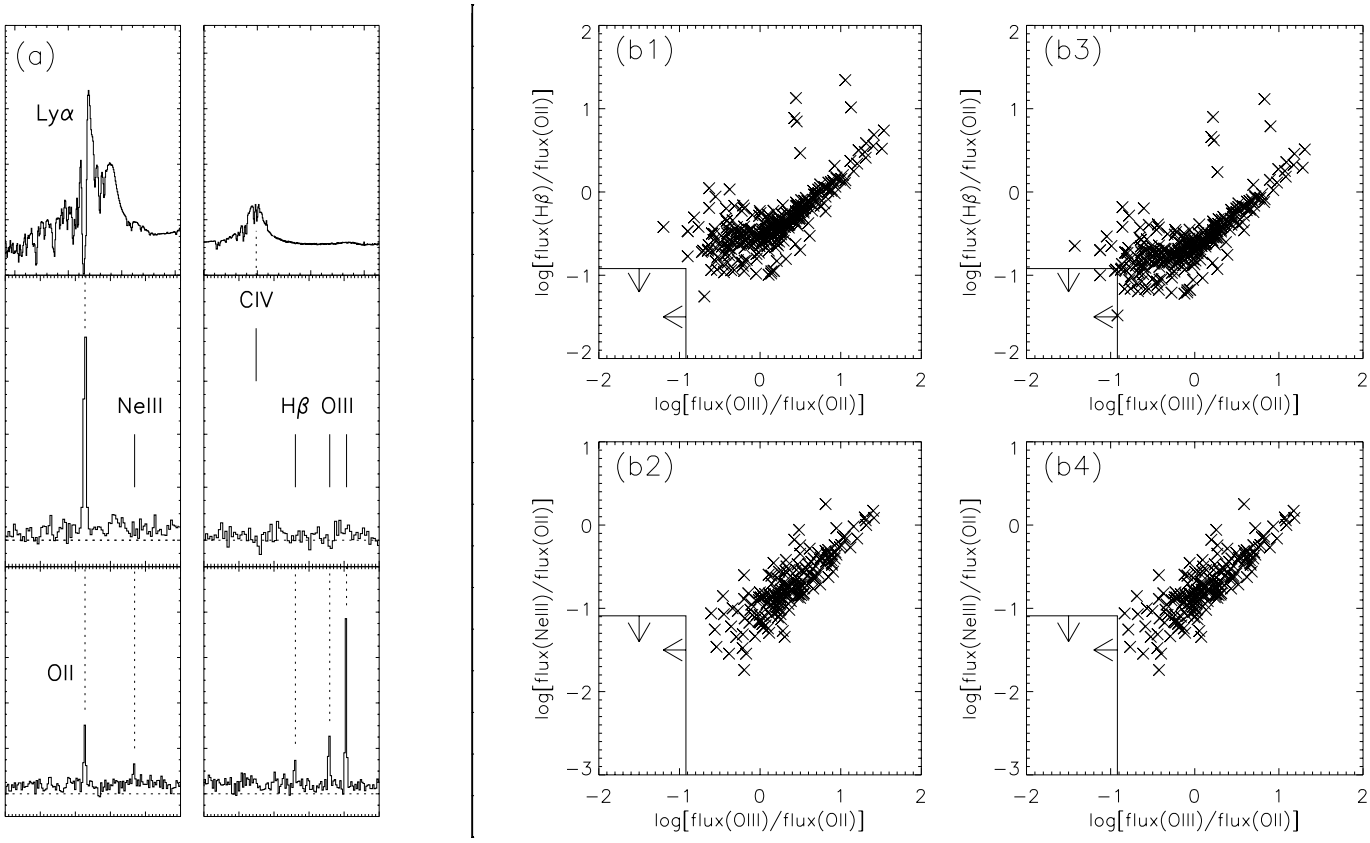

Fig. 5. a) Middle panel shows the stacked G600B (left) and G600R (right) spectrum of S7–S13. Lower panel shows, for comparison, the spectrum of a $z = 0.224$ emission line galaxy redshifted to $z = 0.313$ so that the O II line falls at the wavelength of the observed emission line of S7–S13. The stacked spectrum of S7–S13 has none of the lines expected if S7–S13 had been foreground emission line galaxies. Upper panel shows the spectrum of Q1205-30 to indicate the position of the C IV emission expected for AGNs. A C IV emission line is not detected. **b)** The box to the lower left of each of the figures *(b1,2,3,4)* marks the 2σ limits for the flux ratios $\log(f_{\rm OIII}/f_{\rm OII})$, $\log(f_{\rm H\beta}/f_{\rm OII})$, and $\log(f_{\rm NeIII}/f_{\rm OII})$ under the assumption that S7–S13 are $z = 0.313$ galaxies with O II in the narrow filter. The observed flux ratios from the sample of Terlevich et al. (1991) are plotted ($\times$'s) under two assumptions used for the conversion of equivalent widths to fluxes ("mean" for b1 and b2, and "worst case" for b3 and b4 respectively, see text for details). Under both assumptions the 2σ limits firmly exclude the $z = 0.313$ hypothetis.

where L_ν is the luminosity in the 1500 Å–2800 Å range measured in erg s^{-1} Hz^{-1}. The observed I–band corresponds to the rest-frame UV continuum around 2000 Å, which falls well within this range. We can hence use the I–band flux in the median image of S8, S10–S13 as a measure of their SFRs. To derive L_ν we used the definition of the AB magnitude to derive the observed flux ($F_\nu = 10^{-0.4\times(I({\rm AB})+48.6)}$) and finally the luminosity distance in our assumed cosmology ($d_{\rm lum} = 8.58 \times 10^{28}$ cm) to derive L_ν :

$$\begin{aligned} L_\nu &= F_\nu \times 4\pi d_{\rm lum}^2/(1+z) \\ &= 1.5 \times 10^{28}\,{\rm erg\ s^{-1}Hz^{-1}}, \end{aligned}$$

where the factor $(1+z)^{-1}$ corrects for the fact that L_ν is a specific luminosity (not a bolometric luminosity). Using the relation of Kennicutt (1998) we find a SFR of 2.1 $M_\odot$ yr^{-1}. This is 1–2 orders of magnitude smaller than the SFRs derived for LBGs (Pettini et al. 1998) and 2–3 orders of magnitudes smaller than for the sub–mm selected sources (Ivison et al. 2000).

From the Lyα fluxes we found SFRs for the same objects in the range 0.3–0.5 h^{-2} $M_\odot$ yr^{-1} for a $\Lambda = 0$ cosmology. Converting to the cosmology used in this paper this corresponds to 1.6–2.6 $M_\odot$ yr^{-1}, which is identical to what we now find from the I–band flux. This result is inconsistent with the presence of large amounts of dust in those objects, which is not too surprising as one would expect that a targeted search for Lyα emitters would preferentially find objects with very little or no dust. This *does* however imply that a large number of small star–forming objects at high redshift have essentially no dust in them.

4.3. Space density

The density of Lyα emitters derived from the seven confirmed objects is 16±4 per arcmin^2 per unit redshift (seven objects within the 27.6 arcmin^2 field of view of the EMMI instrument of NTT and within the $\Delta z = 0.016$ range of the narrow filter). In Table 3 we compare this to the results from other recent searches for LEGOs at $z \approx 3$. It is seen from Table 3 that our survey found a larger space

Table 3. The properties of other recent searches for LEGOs at $z \approx 3$.

Survey	z,Δz	Area □'	5σ limit $\times 10^{-17}$ erg s^{-1} cm^{-2}	N	$\frac{dN}{d\Omega dz}$ #/□'	field	Confirmed	Ref.
PKS0528-250	2.81, 0.019	27	3.7	3	5.9 ± 3.4	QSO, DLA	all	(1,2)
HDF N	3.43, 0.063	29	3.0	5	2.7 ± 1.2	blank	all, 2 AGN	(3,4)
SSA 22	3.43, 0.063	30	1.5	7	3.7 ± 1.4	blank	all	(3,4)
BR0019-152	3.43, 0.063	16	-	7	6.9 ± 2.6	blank	3/7	(3,4)
Virgo	3.15, 0.043	50	2.0	9	4.2 ± 1.4	blank	all	(5)
SSA 22a	3.09, 0.066	78	3.0[a]	72	14 ± 1.6	LBG spike	12/72	(6)
Q1205-30	3.04, 0.016	28	1.1	7	16 ± 4	QSO	all	(7)

[a] The true 5σ level for this study is fainter, but only objects brighter than this limit were included in the catalog (Pettini, private communication).
References : (1) Møller & Warren (1993); Warren & Møller (1996); (3) Hu et al. (1998); (4) Cowie & Hu (1998); (5) Kudritzki et al. (2000); (6) Steidel et al. (2000); (7) Fynbo et al. (2000) and this paper.

density than any other survey, but also that we reach the faintest detection limit of them all. The known LBG overdensity studied by Steidel et al. (2000) has a similar space density, but to a three times brighter flux limit. Down to their flux limit we would only have detected two of our seven sources. It is hence not clear from this if the volume around Q1205-30 is overdense in LEGOs, or if we simply see the effect of observing to a lower limiting flux. To be able to address this question, we need to compare our results to the extrapolation of the LBG LF.

Adelberger & Steidel (2000) present a LF for LBG selected galaxies which is based on the HDF–North for the faint ($25 < R < 27$) and ground based LBG surveys for the bright ($R < 25.5$) end. Integrating this LF down to $R = 27$ leads to a predicted density of objects of 0.017 Mpc^{-3} h^3. The comoving volume probed by our survey is 5.8×10^2 Mpc^3 h^{-3}. Based on the LF of LBGs we therefore expect ten galaxies in the volume and we find seven. However, only ∼20% of the Lyman-Break galaxies show Lyα in emission (Steidel et al. 2000). This may be an underestimate if Lyα and continuum emission in general have different spatial distributions due to different slit–losses.

With the Lyman–Break technique the only way to probe the R(AB) > 25.5 part of the LF is to use the Hubble Deep Fields. This makes it impossible at present to study the faint end LF of any significant volume with this technique, and it is therefore very uncertain. Indeed, significant differences in the numbers of high redshift objects in the HDF North and South fields based on photometric redshifts have been reported (Fontana et al. 2000). The faint end of the LF is, however, important to study because a significant fraction of the star–formation, and therefore also the background ionising photons, may originate there. Based on the LF of Adelberger & Steidel (2000) there are roughly equal amounts of total luminosity from galaxies with $R < 25.5$, $25.5 < R < 27$ and $27 < R < 30$. Hence, even if this LF is correct, only about one third of the total star formation at $z = 3$ is traced by the LBGs studied in the ground based samples. In case the faint end LF needs to be revised upwards it will be even less.

Assuming for now that the 20% Lyα fraction can be extrapolated to the faint end of the LF, we find that the volume we have surveyed has a comoving density of faint LBGs which is 3.5 times that predicted by the HDF–North LF. This could indicate that at least some radio quiet QSOs reside in overdense environments. Another likely interpretation is, however, that the faint end of the LF has a larger fraction of Lyα emitters, in our case it must be of order 70% to fit the HDF–North LBG LF. A physical explanation could be that the objects in the faint end of the LBG LF are less dusty that the bright LBGs.

4.4. Redshift distribution

The Lyα emitters were selected in a deep narrow–band search. It now remains to be tested if the objects span the entire width of the narrow–band filter, or if they cluster within a wavelength range smaller than the filter width. The width of the filter response was 23 Å, and the full width spanned by the seven objects is 21.2 Å. Monte Carlo simulations, where we randomly distributed seven objects weighted by the filter transmission curve and measured the resulting mean and std.dev., show that the seven redshifts of S7–S13 are consistent (to within 1σ) with being drawn from a random distribution. Therefore, the structure we have found is most likely larger than the redshift span we have covered with our filter.

5. Conclusions

We have reported on spectroscopic observations of eight candidate Lyα emitting objects at $z \approx 3.04$. All six "certain" ($> 5\sigma$) candidates were confirmed, and of the two "possible" ($< 5\sigma$) candidates one was confirmed. To assess the most likely identification of the lines we performed two independent detailed tests based on a large sample of low redshift O II galaxies. Both tests indicate that the only likely identification is Lyα. This conclusion is strengthened by the fact that the original narrow–band imaging

was centered on a quasar at the same redshift. The seven Lyα objects are hence likely associated with the same structure as the quasar.

The narrow–band images of the objects, as well as the large slit–losses of Lyα emission we need to correct for when calibrating the line fluxes, indicate that the Lyα emission originates in extended objects. This is similar to the results reported by Møller & Warren (1998) on Lyα emission related to a DLA at $z = 2.81$, where it was found that the Lyα emission was significantly more extended than the continuum sources. As these authors point out, this could cause a severe underestimate of the Lyα equivalent widths measured on spectra of high redshift galaxies obtained through a slit.

An analysis of the redshift distribution of the seven confirmed Lyα objects shows that it is consistent with a random distribution in the redshift interval selected via the narrow–band filter.

Despite deep detection limits only S7 and S9 were detected directly in the combined B and I band images. For S8 and S10–S13 we registered the broad band images using the positions of the Lyα sources and determined the median image of the five. This procedure allowed the detection of broad band emission at the level of $B(\mathrm{AB}) \approx 27.3$ and $I(\mathrm{AB}) \approx 26.8$ respectively. This means that S8 and S10–S13 belong to the faint end of the LF at $z = 3$. The derived space density of LEGOs is consistent with the integrated LF of LBGs down to $R = 27$. However, only about 20% of $R < 25.5$ LBGs are Lyα emitters (Steidel et al. 2000). Hence, either the fraction of Lyα emitters at the faint end of the LF is significantly higher than 20% or the space density of galaxies in the field of Q1205-30 is higher than predicted by the LBG LF. The latter would indicate that at least some radio quiet QSOs at high redshift reside in overdense environments.

It has long been argued that Lyα based searches for high redshift galaxies were doomed to failure, because even a small amount of dust would quench the Lyα emission due to the resonant scattering of the Lyα photons. For this reason it has been virtually impossible to obtain telescope time for Lyα survey work. We note here in passing that the recent very successful Lyα survey by Kudritzki et al. (2000) was aimed at low redshift planetary nebulae, and the work that supplied our candidate list was aimed at the imaging of a quasar absorber. It is virtually certain that neither of those programmes had been granted telescope time if the aim had been to search for a sample of Lyα emitters at $z = 3$.

In this paper we find two strong arguments against the presence of significant amounts of dust in the objects in the faint end of the high redshift galaxy LF. Firstly we find very large equivalent widths, in the upper range of theoretical predictions. Secondly we find that when we calculate the star–formation rate from the continuum flux and from the Lyα flux independently, we obtain identical results. Both of those observations are inconsistent with a dust–rich environment.

The faint continuum magnitudes detected for S8 and S10–S13 prove that Lyα emission is a powerful method by which to probe the faint end of the galaxy LF at $z \sim 3$. The next step is now to obtain statisitically significant samples, containing several hundred Lyα selected galaxies, in order to further constrain the properties of the faint end of the luminosity function.

Acknowledgements. We are grateful for excellent support during our service observations in January and during the observing run on Paranal in March. We thank the referee A. Fontana for several comments that clarified our manuscript on important points.

References

Adelberger, K., & Steidel, C. C. 2000, ApJ, 544, 218
Cowie, L. L., & Hu, E. M. 1998, AJ, 115, 1319
Bloom, J. S., Odewahn, S. C., Djorgovski, S. G., et al. 1999, ApJ, 518, L1
Charlot, S., & Fall, S. M., ApJ, 415, 580
Efstathiou, G. 2000, MNRAS, 317, 697
Ellison, S. L., Pettini, M., Steidel, C. C., & Shapley, A. E. 2001, ApJ, 549, 770
Fontana, A., D'Odorico, S., Poli, F., et al. 2000, AJ, 120, 2206
Francis, P. J., Woodgate, B. E., Warren, S. J., et al. 1995, ApJ, 457, 490
Fynbo, J. U., Møller, P., & Warren, S. J. 1999, MNRAS, 305, 849
Fynbo, J. U., Thomsen, B., & Møller, P. 2000, A&A, 353, 457 (Paper I)
Fynbo, J. U., Gorosabel, J., Dall, T., et al. 2001, A&A, 373, 796
Haehnelt, M. G., Steinmetz, M., & Rauch, M., ApJ, 534, 594
Haehnelt, M. G., Madau, P., Kudritzki, R.-P., & Villamariz, M. R. 2001, A&A, 549, L151
Hogg, D. W., & Fruchter, A. S. 1999, ApJ, 520, 54
Holland, S., & Hjorth, J. 1999, A&A, 344, L67
Hu, E. M., Cowie, L. L., & McMahon, R. G. 1998, ApJ, 502, L99
Ivison, R. J., Smail, I., Barger, A. J., et al. 2000, MNRAS, 315, 209
Jensen, B. L., Fynbo, J. U., Gorosabel, J., et al. 2001, A&A, 370, 909
Kennicutt, R. C. 1998, ARA&A, 36, 189
Kudritzki, R.-P., Méndez, R. H., Feldmeier, J. J., et al. 2000, ApJ, 536, 19
Kulkarni, V. P., Hill, J. M., Schneider, G., et al. 2000, ApJ, 536, 36
Kulkarni, V. P., Hill, J. M., Schneider, G., et al. 2000, ApJ, 551, 37
Kurk, J. D., Röttgering, H. J. A., Pentericci, L., et al. 2000, A&A, 358, L1
Møller, P., & Warren, S. J. 1993, A&A, 270, 43
Møller, P., & Warren, S. J. 1998, MNRAS, 299, 661
Møller, P., & Fynbo, J. U. 2001, A&A, 372, L57
Odewahn, S. C., Djorgovski, S. G., Kulkarni, S. R., et al. 1998, ApJ, 509, L5
Pascarelle, S. M., Windhorst, R. A., Driver, S. P., Ostrander, E. J., & Keel, W. C. 1996, ApJ, 456, L21

Pascarelle, S. M., Windhorst, R. A., & Keel, W. C. 1998, AJ, 116, 2659
Pentericci, L., Kurk, J. D., Röttgering, H. J. A., et al. 2000, A&A, 361, L25
Pettini, M., Kellogg, M., Steidel, C. C., et al. 1998, ApJ, 508, 539
Poli, F., Menci, N., Giallongo, E., et al. 2001, ApJ, 551, L45
Rauch, M., Steinmetz, M., & Haehnelt, M. 1997, ApJ, 481, 601
Rhoads, J. E., Malhotra, S., Dey, A., et al. 2000, ApJ, 545, L85
Roche, N., Lowenthal, J., & Woodgate, B. 2000, MNRAS, 317, 937
Smette, A., Fruchter, A. S., Gull, T. R., et al. 2001, ApJ, in press [astro-ph/0007202]
Steidel, C. C., & Hamilton, D. 1992, AJ, 104, 941
Steidel, C. C., Giavalisco, M., Pettini, M., Dickinson, M., & Adelberger, K. 1996, ApJ, 462, L17
Steidel, C. C., Adelberger, K., Shapley, A. E., et al. 2000, ApJ, 532, 170
Steidel, C. C., Pettini, M., & Adelberger, K. 2001, ApJ, 546, 665
Stern, D., Bunker, A., Spinrad, H., & Dey, A. 2000, ApJ, 537, 73
Terlevich, R., Melnick, J., Masegosa, J., Moles, M., & Copetti, M. V. F. 1991, A&AS, 91, 285
Thacker, R. J., & Couchman, H. M. P. 2000, ApJ, 545, 728
Valls-Gabaud, D. 1993, ApJ, 419, 7
Vreeswijk, P. M., Fruchter, A., Kaper, L., et al. 2001, ApJ, 546, 672
Warren, S. J., & Møller, P. 1996, A&A, 311, 25
Warren, S. J., Møller, P., Fall, S. M., & Jakobsen, P. 2001, MNRAS in press [astro-ph/105032]